

1 **Rational design, supramolecular synthesis and solid state characterization of two**
2 **bocimponent solid forms of Mebendazole**

3 Eduardo L. Gutiérrez¹, Agustín A. Godoy², Griselda E. Narda² and Javier Ellena^{3,*}

4 ¹INQUISAL–CONICET, San Luis, Argentina – Área de Química Física, Facultad de Química, Bioquímica y Farmacia,
5 Universidad Nacional de San Luis. Chacabuco y Pedernera 5700, San Luis, Argentina.

6 ²Instituto de Investigaciones en Tecnología Química (INTEQUI), Almt. Brown 1500-1402, D5700APA, San Luis –
7 Área de Química General e Inorgánica “Dr. G. F. Puelles”, Facultad de Química, Bioquímica y Farmacia, Universidad
8 Nacional de San Luis, Chacabuco y Pedernera, 5700 San Luis, Argentina.

9 ³Instituto de Física de São Carlos, Universidade de São Paulo, CP 369, 13.560-970, São Carlos, SP, Brazil.

10 * e-mail address: javiere@ifsc.usp.br

11

12

13

14

15

16

17

18

19

20

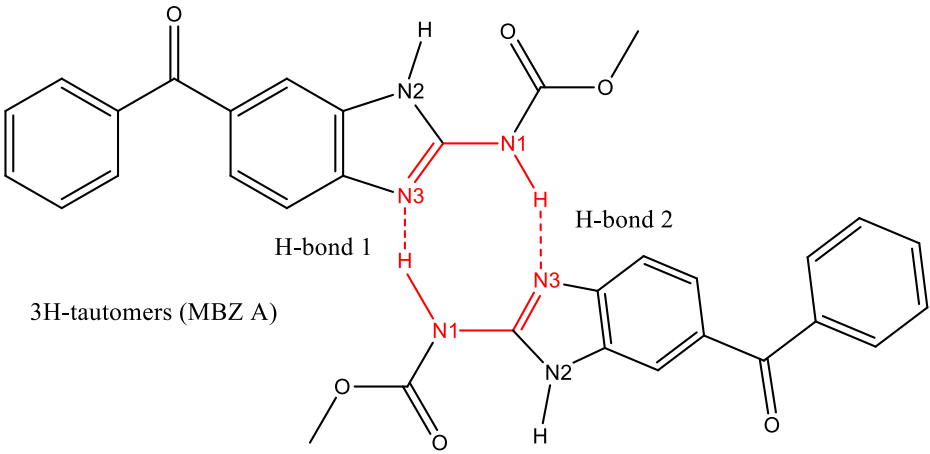
21

22

23

24

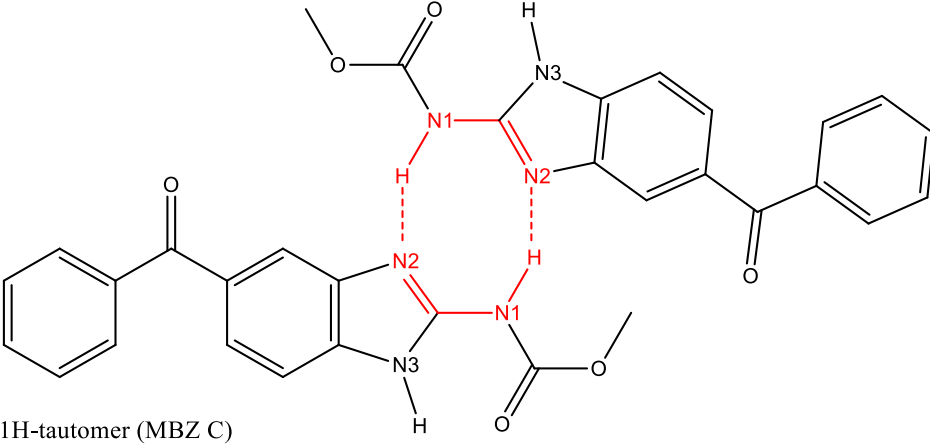
25

Table S1. MBZ...MBZ $R_2^2(8)$ homosynthon found in MBZ A


3H-tautomers (MBZ A)

	H-bond 1		H-bond 2	
	A...H / Å	A...D / Å	A...H / Å	A...D / Å
MBZ A ¹	2.1	2.86(3)	2.1	2.86(3)

¹ F. F. Ferreira, S. Antonio Gutierrez, P. C. Pires Rosa and C. de O. Paiva-Santos, *Int. J. Drug Dev. Res.*, 2011, **3**, 26–33.

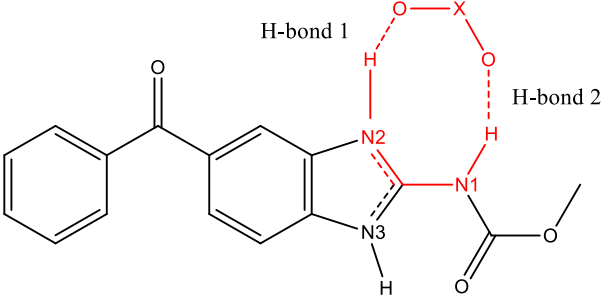
Table S2. MBZ...MBZ $R_2^2(8)$ homosynthon found in MBZ C


1H-tautomer (MBZ C)

	H-bond 1		H-bond 2	
	A...H / Å	A...D / Å	A...H / Å	A...D / Å
MBZ C ²	1.99	2.872(8)	1.99	2.872(8)

² F. T. Martins, P. P. Neves, J. Ellena, G. E. Camí, E. V. Brusau and G. E. Narda, *J. Pharm. Sci.*, 2009, **98**, 2336–2344.

Table S3. $R_2^2(8)$ heterosynthons involving **N1** and **N2** found in some MBZ salts (including the two reported in this work)



Salts	X	H-bond 1		H-bond 2	
		A...H / Å	A...D / Å	A...H / Å	A...D / Å
MBZ / perchloric acid	Cl	1.94	2.785(5)	2.04	2.875(5)
MBZ / methylsulfuric acid	S	1.89	2.742(3)	1.90	2.736(3)
MBZ / nitric acid ³	N	1.87	2.720(2)	2.08	2.759(3)
MBZ / formic acid* ⁴	C	1.79	2.664(5)	1.95	2.793(5)
		1.84	2.704(5)	1.90	2.779(5)
		1.79	2.658(5)	1.90	2.777(5)
MBZ / methyloxalic acid ⁵	C	1.50	2.598(3)	2.01	2.798(4)

*MBZ formate presents three different heterosynthons of this tipe.

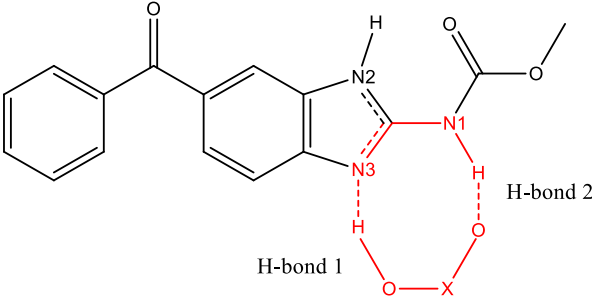
³ E. L. Gutiérrez, M. S. Souza, L. F. Diniz and J. Ellena, *J. Mol. Struct.*, 2018, **1161**, 113–121.

⁴ J.-M. Chen and T. Lu, *Chinese J. Chem.*, 2013, **31**, 635–640.

⁵ J.-M. Chen, Z.-Z. Wang, C.-B. Wu, S. Li and T.-B. Lu, *CrystEngComm*, 2012, **14**, 6221.

31
32
33
34
35
36
37
38
39
40
41
42
43
44

Table S4. $R_2^2(8)$ heterosynthon involving **N1** and **N3** found in some MBZ salts and cocrystals



System	X	Neutral/ionic Status*	H-bond 1		H-bond 2	
			A...H / Å	A...D / Å	A...H / Å	A...D / Å
MBZ / trifluoroacetic acid ⁴	C	salt	1.79	2.650(2)	1.80	2.672(2)
MBZ / acetic acid ⁴	C	cocrystal	1.88	2.689(2)	1.91	2.753(2)
MBZ / propionic acid ⁶	C	cocrystal	1.70	2.664(5)	1.80	2.787(4)
MBZ / butyric acid ⁴	C	cocrystal	1.84	2.660(2)	1.95	2.793(2)
MBZ / valeric acid ⁴	C	cocrystal	1.85	2.660(2)	1.98	2.820(2)
MBZ / caproic acid ⁴	C	cocrystal	1.87	2.705(3)	1.90	2.762(3)
MBZ / glutaric acid ⁵	C	cocrystal	1.71	2.690(2)	1.90	2.764(2)
MBZ / maleic acid ** ⁵	C	salt	1.63	2.608(4)	1.95	2.790(4)
			1.72	2.627(4)	1.71	2.757(4)

* Ionic status (salts) implies that both **N1** and **N3** act as donors (H-bond 1 is: **N3-H**...**O**).

** *MBZ maleate presents two different heterosynthons of this type.

⁴ J.-M. Chen and T. Lu, *Chinese J. Chem.*, 2013, **31**, 635–640.

⁵ J.-M. Chen, Z.-Z. Wang, C.-B. Wu, S. Li and T.-B. Lu, *CrystEngComm*, 2012, **14**, 6221.

⁶ M. Caira, T. Dekker and W. Liebenberg, *J. Chem. Crystallogr.*, 1998, **28**, 11-15.

45

46

47

48

49

50

51

52

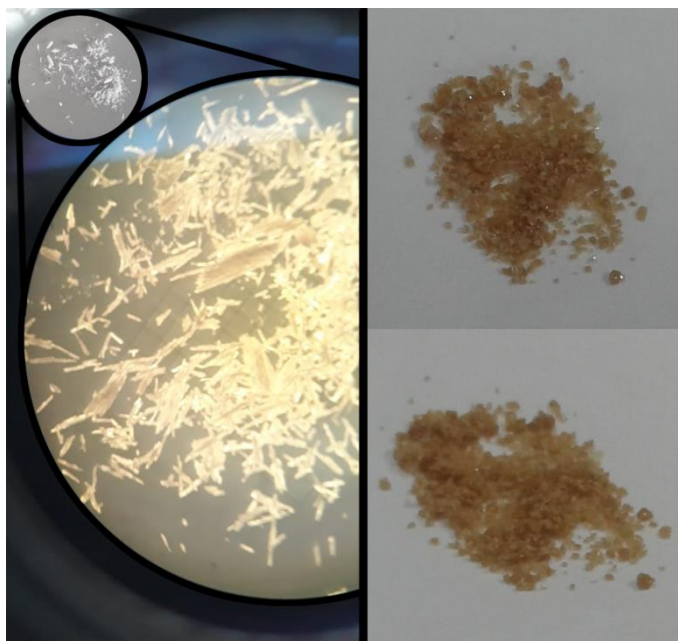
53

54

55

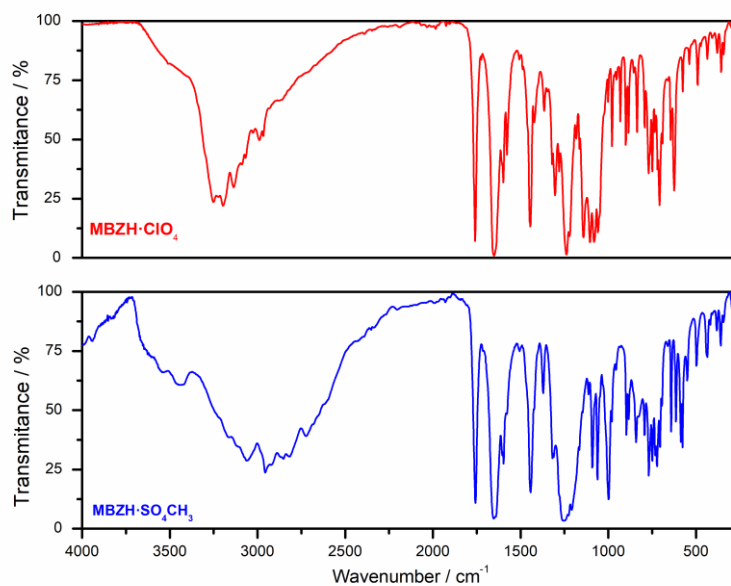
56 Results and discussion

57 *Crystalline habit, identity and purity*



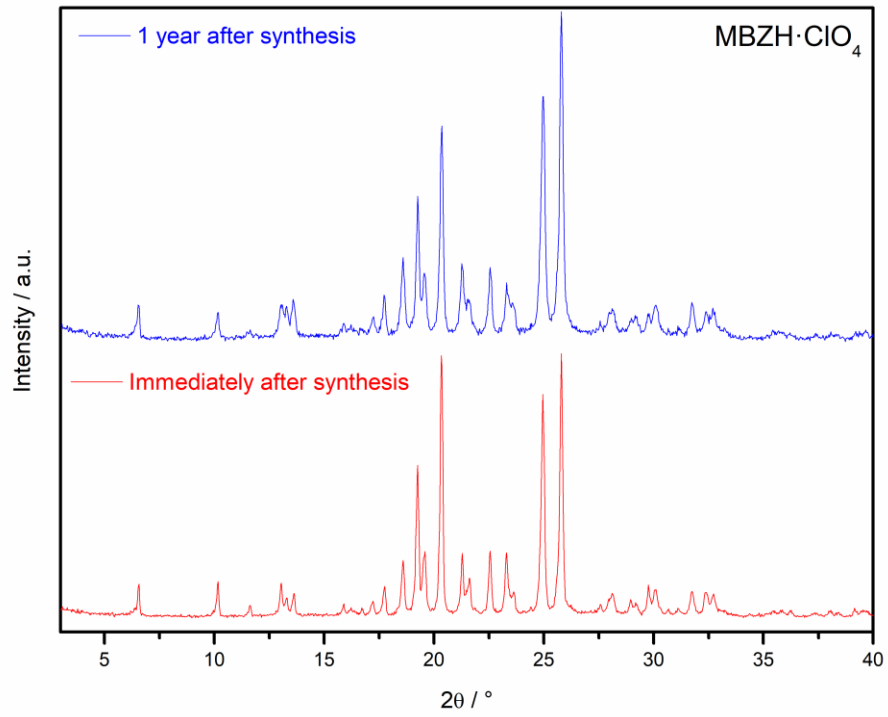
58

59 **Figure S1.** Left: MBZ methylsulfate crystals. Right: MBZ perchlorate crystals.



60

61 **Figure S2.** FT-IR spectra of MBZ perchlorate and MBZ methylsulfate.



62

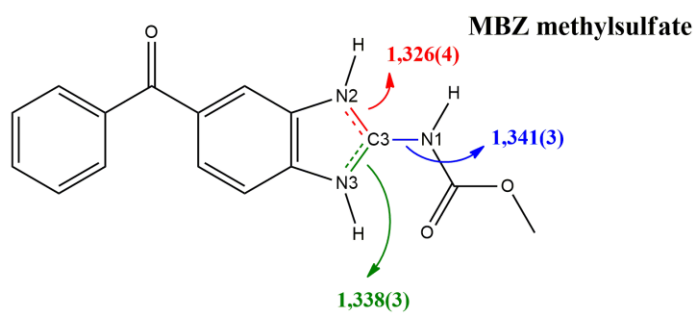
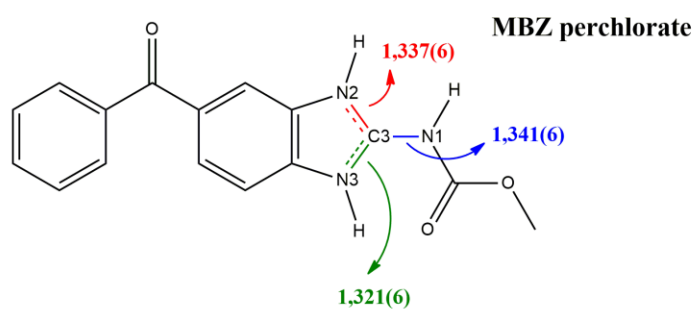
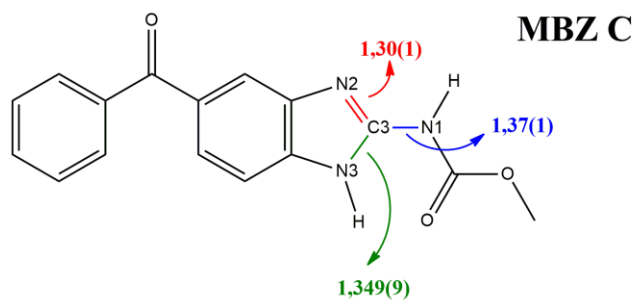
63 **Figure S3.** Comparison of Power X-ray diffraction patterns of MBZ perchlorate immediately after the synthesis and

64

one year after the synthesis.

65

66



67

68

Figure S4. Effect of protonation on bond lengths of MBZ molecule.

69

70

71

72

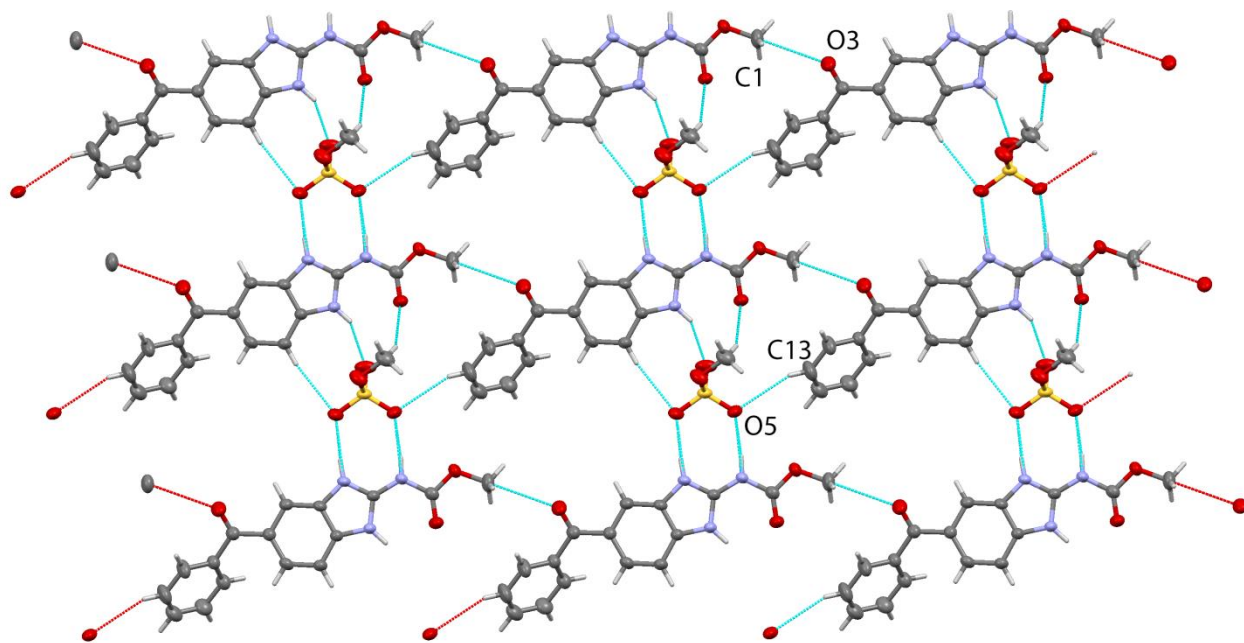
73

74

75

76

77



78

79 **Figure S5.** One non-classical H-bond between **O5** and **C13** ($A\cdots H$: 2.68 Å), and one interaction between
 80 the bezoylic **O3** of one $MBZH^+$ and **C1** of next cation (3.213(4) Å), give rise to infinite layers parallel to a
 81 axis. (Color code. C: grey; H: white; O: red; N: blue; S: yellow.)

82

83

84

85

86

87

88

89

90

91

92

93

94

95

96

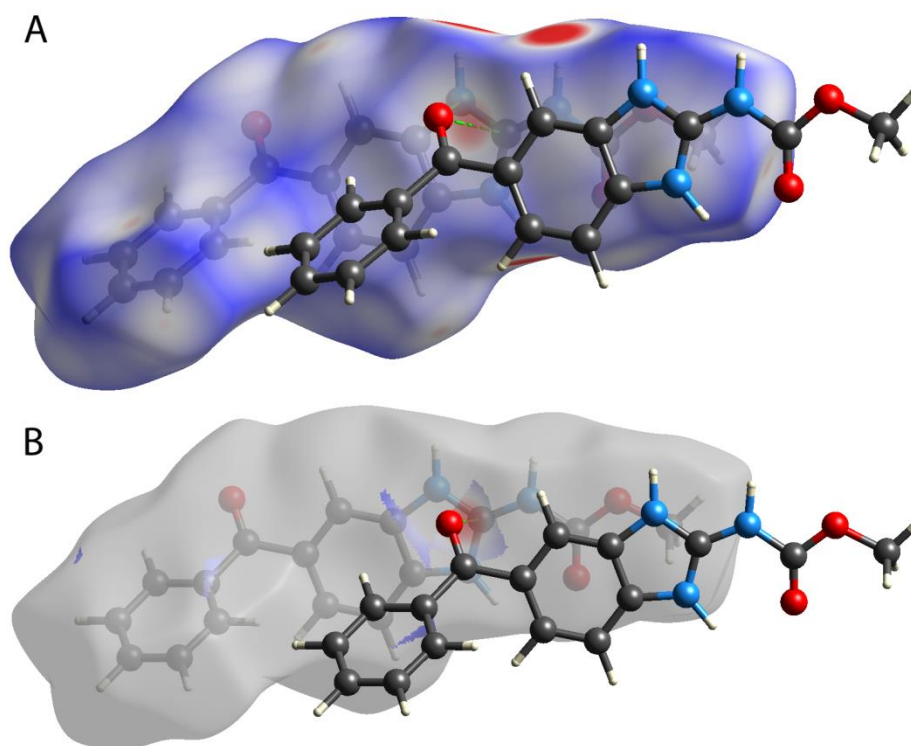
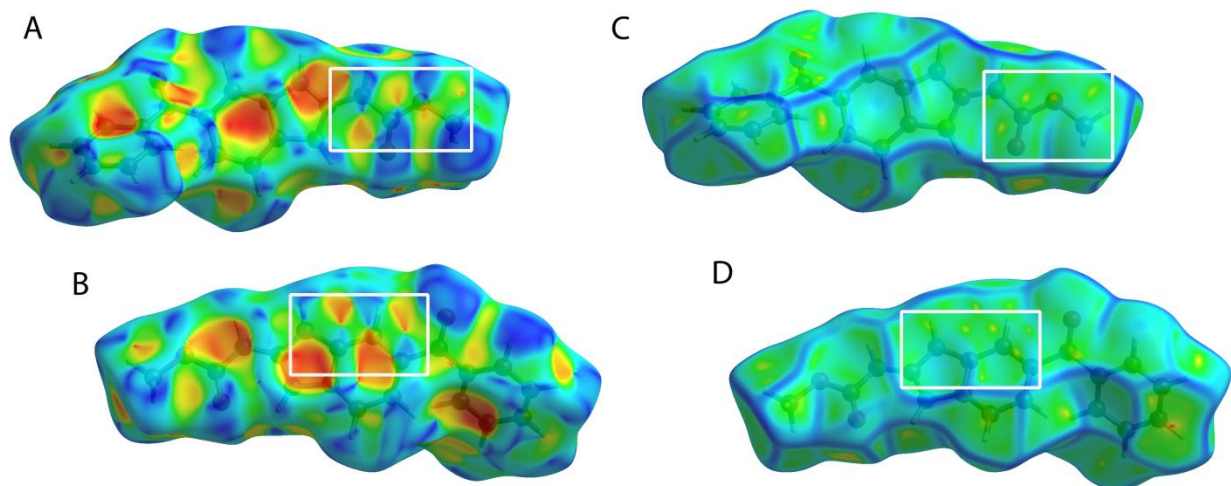


Figure S6. Short contacts $N2 \cdots O3$ and $C3 \cdots O3$ shown over d_{norm} surface.

103 **Figures S8A & B** show the 2D-fingerprint plots of $MBZH \cdot ClO_4$ and $MBZH \cdot SO_4CH_3$. The dominant interaction
104 in both structures is the cyclic H -bonded $R_2^2(8)$ heterosynthon. This interaction shows up as a pair of spikes at the
105 bottom left of the plot (orange ellipsoids). The asymmetry in these spikes is due to the fact that in the $R_2^2(8)$
106 arrangement both N atoms from $MBZH^+$ act as donors and both O from ClO_4^- act as acceptors. The small
107 contribution to the small spike corresponds to the O atoms of $MBZH^+$ acting as acceptors non-classical weaker
108 interactions. Although both fingerprint plots are quite similar, an important difference due to the presence of $C \cdots C$
109 interactions in $MBZH \cdot ClO_4$ is present. These interactions giving rise to a stacking arrangement are revealed by the
110 density of bins in the center of the plot as a green region (red ellipsoid in **Figures S8A**). In Figure **Figures S8C** we

111 show the histograms representing the relative areas of the d_{norm} surface partitioned between the different types of
112 interactions. $H\cdots O/O\cdots H$ are the main interactions found in both salts (35.5 % in $MBZH\cdot ClO_4$ and 32.2 % in
113 $MBZH\cdot SO_4CH_3$), follow by $H\cdots H$ and $C\cdots H/H\cdots C$ interactions (27.2 % and 32.4 %, and 19.6 % and 20.2 %
114 respectively).

115

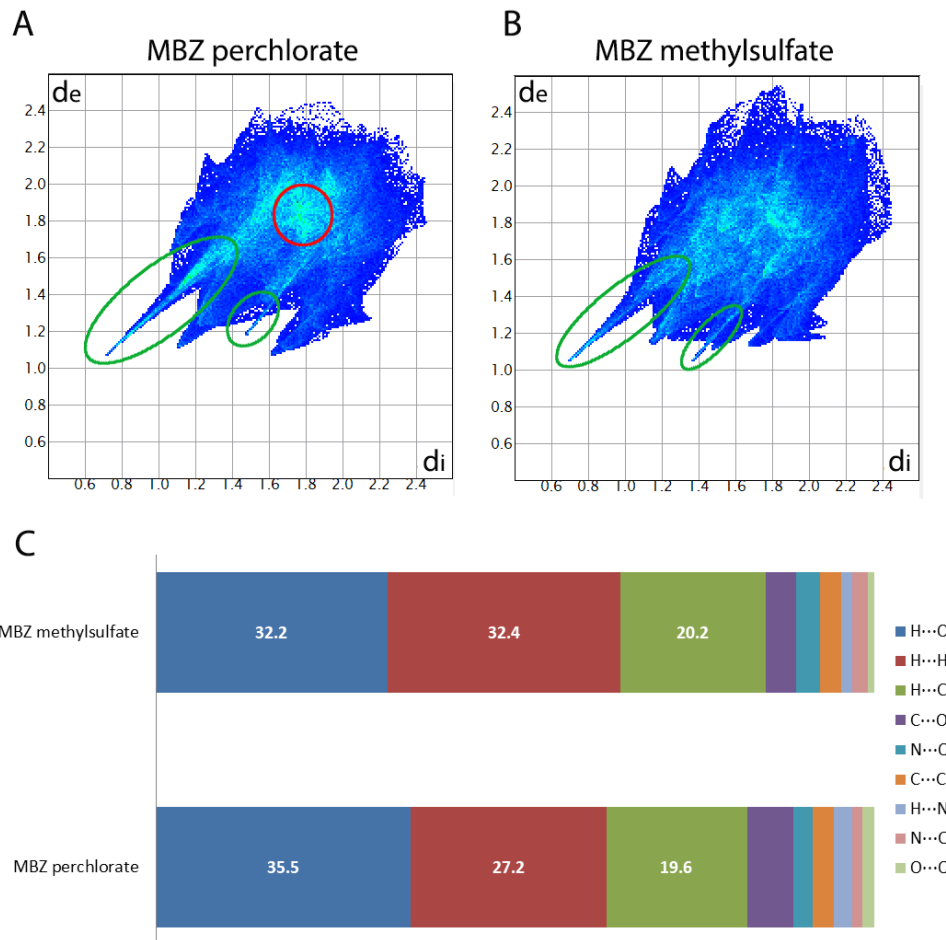


116

117 **Figure S7.** Shape index surface (A & B) and Curvedness surface (C & D) over MBZH+ on $MBZH\cdot ClO_4$.

118

119



120

121 **Figure S8.** 2D-fingerprint plots of MBZH·ClO₄ (**A**) and MBZH·SO₄CH₃ (**B**). **C:** histograms representing the relative

122 areas of the d_{norm} surface partitioned between the different types of interactions.

123

124

125

126

127

128

129

130 *Thermal stability*

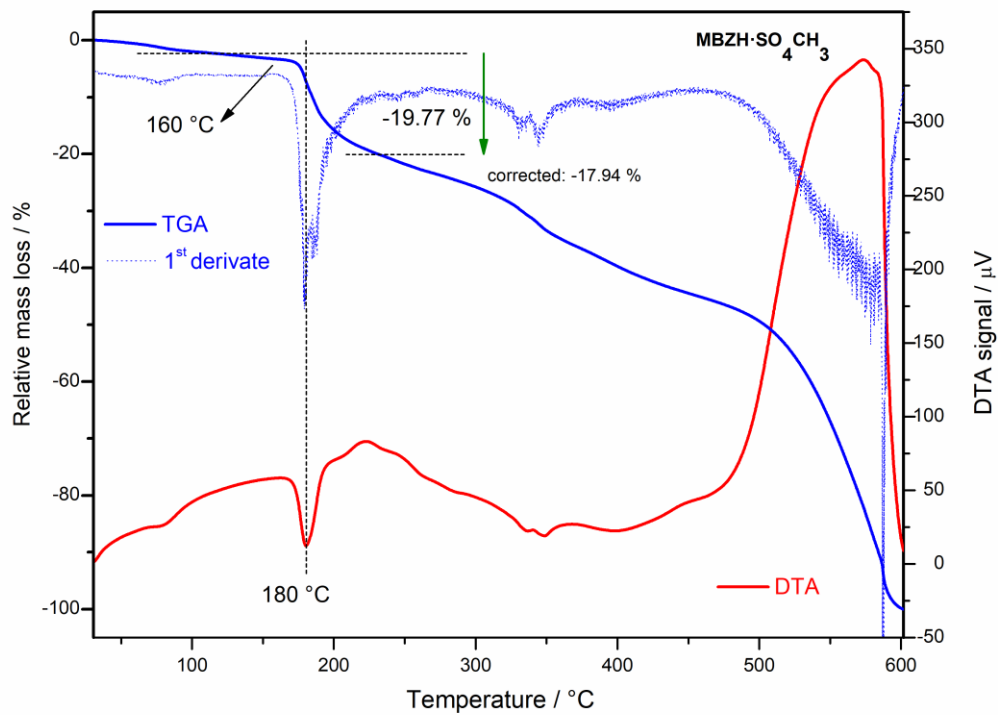
131 In the mechanism proposed by Holanda *et al.*, MBZ decompose with the release of CH₃OH and carbon
132 monoxide (CO). The following reaction of CO with O₂ to produce carbon dioxide (CO₂) could be interpreted as the
133 driving force for the decomposition reaction of the drug. A rather different mechanism was proposed by Roque-
134 Flores *et al.* for the decomposition of MBZ in N₂ atmosphere that involves an intramolecular rearrangement
135 through a six-membered ring intermediate which allows the transposition of the methyl group from the ester
136 moiety towards the pyridinic N of imidazole ring. In this case, the first product of MBZ decomposition is 2-amino-1-
137 methyl-5-benzoylbenzimidazole. This particular mechanism cannot operate for MBZ salts since both imidazole
138 nitrogen atoms are protonated and the transposition cannot occur. The disappearance of the methyl C–H
139 stretching modes bands at 2990 cm⁻¹ and 2967 cm⁻¹ in the temperature-variable FT-IR spectra seems to indicate
140 that the transposition mechanism proposed by Roque-Flores *et al.* does not operate here.

141 A second stage of the thermal decomposition of MBZH·ClO₄ starts almost immediately (260 °C) and seems
142 to involve two overlapped exothermic events with a relative mass loss of 29.00 %. **Scheme S1** shows the propose
143 decomposition mechanism in which the cleavage of the amine bond with the removal of ammonia is followed by
144 the subsequent elimination of perchloric acid. Theoretical mass loss for these consecutives eliminations is 29.18 %,
145 in good agreement with the experimental value. The final stage is the complete degradation of the remaining
146 compound, 5-benzoylbenzimidazole.

147

148

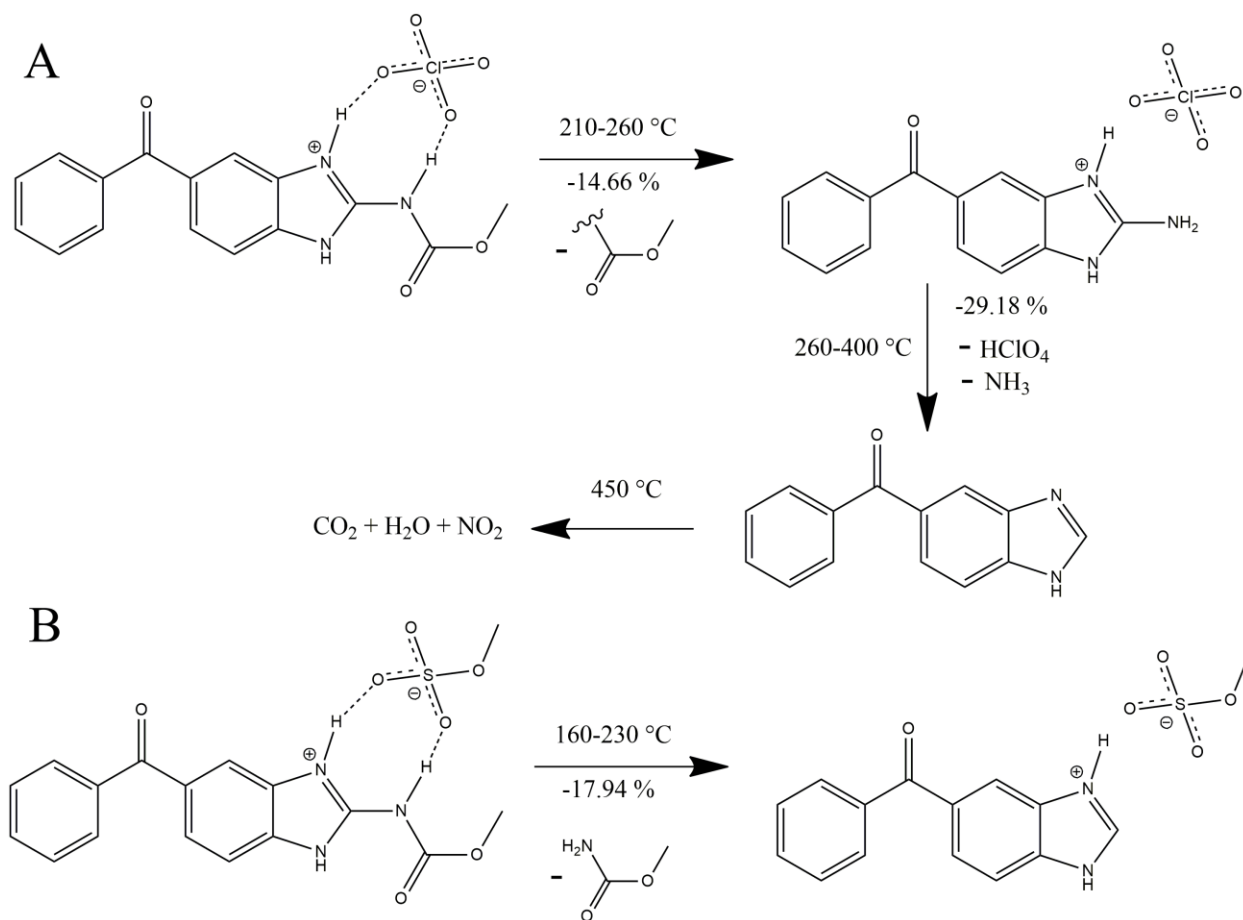
149



150

151

Figure S9. TGA and DTA curves of MBZ methylsulfate.



152

153 **Scheme S1.** Proposed mechanisms for MBZ perchlorate (**A**) and MBZ methylsulfate (**B**) thermal degradation.

154

155

156

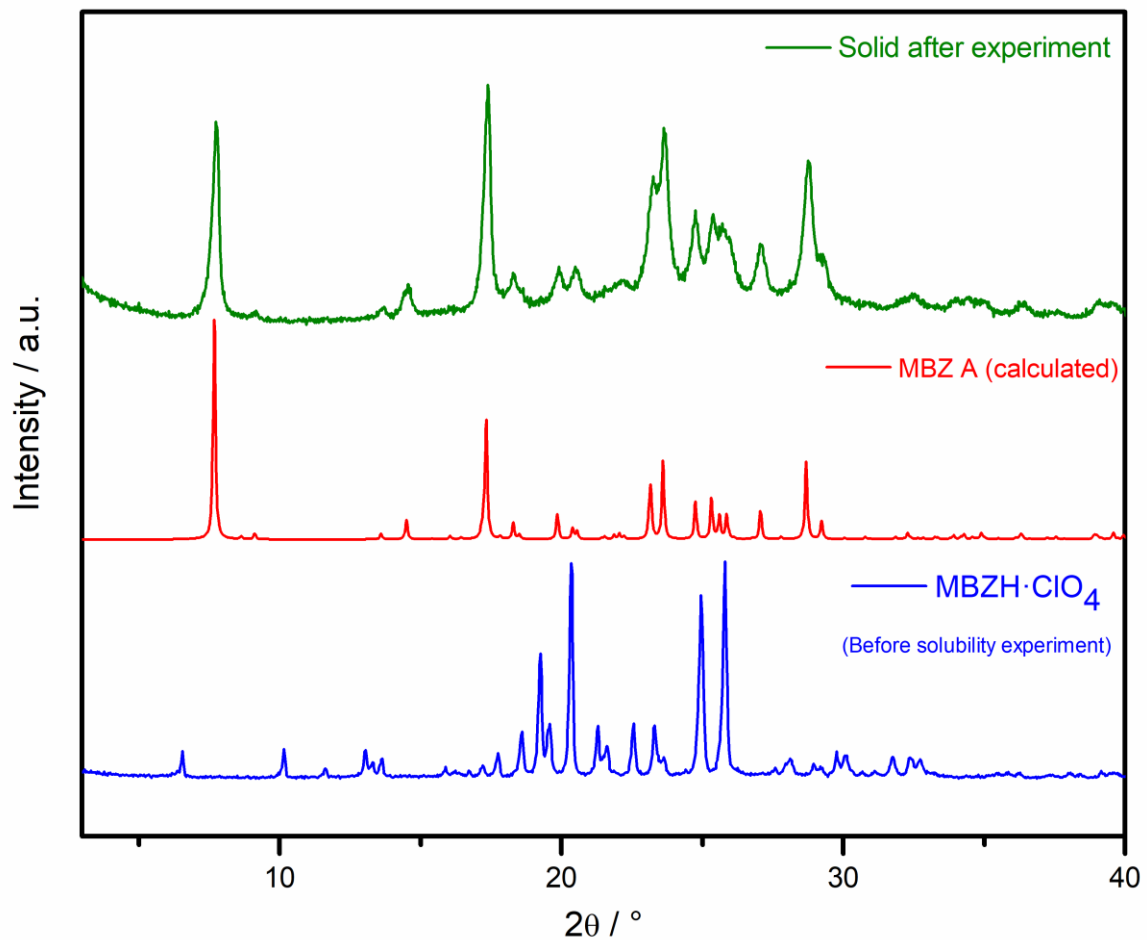
157

158

159

160

161



165 **Figure S10.** Power X-ray diffraction patterns of the solids before and after the solubility experiment, compared with
166 the calculated pattern of MBZ A.